

Artificially ordered Fe-Cu alloy superlattices on Cu(001). I. Studies on the structural and magnetic properties

S. Sundar Manoharan,* M. Klaua, J. Shen, J. Barthel, H. Jenniches, and J. Kirschner
Max-Planck Institut für Mikrostrukturphysik, Weinberg 2, Halle (Saale), D-06120, Germany

(Received 9 March 1998)

Metastable fcc Fe-Cu alloys in the $L1_0$ phase have been prepared by stacking one monolayer of Fe and one monolayer of Cu alternately, $[\text{Fe}(1 \text{ ML})/\text{Cu}(1 \text{ ML})]_n$ (where $n \leq 25$) onto a Cu(001) substrate using pulsed-laser deposition. The observed reflection high-energy electron-diffraction oscillations for each Fe and Cu layer and their growth mode as studied by scanning tunneling microscopy indicate a nearly layer-by-layer growth. Alloys up to $n = 22$ (22 bilayers) have fcc(001) structure, then change from fcc to bcc structure. Magnetic hysteresis loops measured using the magneto-optical Kerr effect indicate that for $1 \leq n \leq 25$ the films are ferromagnetic with the easy axis of magnetization within the plane of the films. For the basic unit of double-layer configuration a Curie temperature of 130 K is estimated. It increases linearly with the number of stackings reaching a saturation value of 400 K at five double layers and beyond. [S0163-1829(98)03637-6]

INTRODUCTION

Artificially grown, magnetic monatomic multilayers such as Fe-Au,¹ Fe-Pt,² and Fe-Cu (Ref. 3) systems are the low thickness limit of a multilayer, consisting of alternate layers of magnetic and nonmagnetic elements. Alternatively, they may be viewed as ordered 1:1 alloys with a certain crystalline structure. Alloying effects on magnetism of transition metals has been a subject of long standing interest.^{4,5} In many cases, the magnetic moment of the Fe atom is quickly reduced by alloying and the alloy system becomes nonmagnetic. Experimental work on the extended miscibility of the Fe-Cu system was performed on bulk solid samples *rapidly quenched* from elevated temperatures.⁶ These studies were successful in stabilizing up to 15 at. % of Cu in the bcc Fe matrix.⁷ The measured lattice parameters of these alloys were shown to increase nearly linearly with the Cu content following Vegard's law.⁸

Earlier observations on the FeCu alloy

Numerous efforts have been undertaken to stabilize solid solutions of Fe in Cu and *vice versa*. In the equilibrium state, Fe and Cu have very small mutual solid solubility and form no intermetallic compounds, even though their atomic radii are quite similar. This behavior is in accordance with the positive value of the calculated heat of mixing between Fe and Cu. However, by using *vapor-quenching* methods^{9,10} such as sputtering, which bypass the liquid phase, the solid miscibility can be extended, and a metastable FeCu solid solution can be formed over the entire range of composition. It has been reported that the Fe-rich samples are bcc and ferromagnetic. Alloys with more than 70% Cu are fcc and appear to be paramagnetic. At elevated temperatures the alloys decompose into a Fe-rich bcc phase and a Cu-rich fcc phase. Samples of $\text{Fe}_x\text{Cu}_{100-x}$ produced by *high rate sputtering* indicate Fe-rich samples for $x > 75$ to be in the bcc structure, while the samples with $x < 60$ are in the fcc structure.

In the past few years, much research has been performed on metastable FeCu alloys prepared via *high-energy ball milling*¹¹⁻¹³ (HEBM) since it was shown that by this means the solubility of Fe in fcc Cu can be extended up to $\cong 60$ at. %. This technique offers an alternative to rapid quenching techniques. Uenishi *et al.*¹⁴ report that the lattice parameters of bcc and fcc HEBM metastable FeCu alloys increase nearly linearly with increasing concentration of the dilute elements, i.e., Cu in bcc Fe and Fe in fcc Cu reaching a maximum for $\text{Cu}_{50}\text{Fe}_{50}$. The same authors also have shown¹⁵ that the volume expansion is significantly larger in HEBM samples than in sputtered material indicating that the local structure must be different from those FeCu alloys produced by quenching techniques. The alloying phenomenon in these latter materials has been explained by Yavari, Desre, and Benameur¹⁶ to arise when small fragments obtain a critical tip radius, where capillary forces bring about the dissolution of the tip region, and the eventual mixing of one component into the other.

Epitaxial growth of alloys

In contrast to the above-mentioned techniques which are producing *polycrystalline* or *amorphous* metastable alloys, a particular composition like $\text{Fe}_{50}\text{Cu}_{50}$ can be grown as a *single crystalline* ordered alloy by means of epitaxially stacking monolayers of Fe and Cu alternately onto an appropriate substrate. Recent development of sophisticated growth techniques like pulsed-laser deposition (PLD) has made it possible to fabricate materials that do not exist in nature. The $\text{Fe}_{50}\text{Cu}_{50}$ alloy is such a system which is thermodynamically unstable in bulk as inferred from the Fe-Cu phase diagram near the equiatomic composition.¹⁷

In general, the feasibility of fabricating any epitaxial alloy system depends on the bulk properties of the constituent elements. If the lattice misfit is not too large, epitaxy makes it possible to stabilize γ -Fe (fcc) phase which otherwise exists only above 1184 K. A Cu(001) single crystal is the substrate of choice for pseudomorphic fcc Fe because a small negative

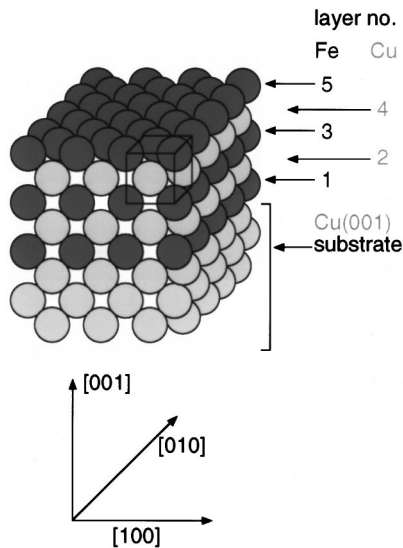


FIG. 1. Scheme of Fe and Cu monolayer stacking on Cu(001) in the $L1_0$ structure. Note the evolution of the fcc FeCu alloy as we increase the number of monolayers. Cu, respectively, Fe is on top of the stack at every even, respectively, odd total number of monolayers.

misfit ($\approx -1\%$) forces an increased lattice spacing. According to the *ab initio* electronic structure calculation¹⁸ an increased lattice constant may stabilize a ferromagnetic ground state in the otherwise antiferromagnetic fcc Fe.

Another aspect of great relevance in constructing an FeCu epitaxially ordered alloy is the two-dimensional (2D) growth mode. However, from thermodynamic reasons of surface and interface energies one cannot expect 2D growth. Even the kinetics of the normal thermal deposition have proved to be insufficient to overcome the thermodynamic limitation as it has been reported.¹⁹ In view of this, it is not surprising that the growth of Fe on Cu is experimentally difficult. While thermal deposition of Fe on Cu(001) does not produce an ideal 2D growth at monolayer thickness,²⁰ its morphology can be significantly improved by PLD.²¹ The momentaneous deposition rate of PLD (which is typically 10^5 to 10^6 times larger than that of the thermal deposition) provides a high nucleation density thereby supporting 2D layer-by-layer growth of Fe on Cu(001). Since a layer-by-layer growth is an essential prerequisite to construct such stacked Fe-Cu monatomic multilayers, the PLD technique here is the method of choice.

In this paper we present a detailed investigation on the fabrication of monolayer superlattices of the ordered $L1_0$ phase of Fe and Cu deposited alternately on a Cu(001) substrate (Fig. 1) at room temperature (RT) using pulsed-laser deposition. The growth, morphology, and structure evolution as the stacking increases will be presented based on reflection high-energy electron-diffraction (RHEED), scanning tunneling microscopy (STM), and low-energy electron-diffraction (LEED) studies, respectively. The magnetic properties have been monitored by magneto-optical Kerr effect (MOKE) measurements. Spin-resolved electronic properties and magnetic dichroism measurements are the subject of a future paper.³¹

GROWTH AND MORPHOLOGY

Growth conditions

The growth of each monolayer of Fe and Cu was monitored by means of typical RHEED oscillations (at 34 keV beam energy with a glancing angle of about 2.5° in $\langle 100 \rangle$ incidence). The Fe-Cu multilayers were grown on a Cu(001) substrate (miscut $\leq 0.1^\circ$) at room temperature in an ultrahigh vacuum system with a base pressure of 3×10^{-11} mbar equipped with facilities for *in situ* RHEED, MOKE, STM, and LEED. Care was taken to clean the Cu(001) substrate with cycles of Ar^+ sputtering and annealing at 600°C until an average terrace width of about 300 nm (locally varying between 50 and 500 nm) was achieved as proven by STM without any measurable quantities of contaminants by Auger electron spectroscopy.²²

Prior to depositing monolayers of Fe and Cu, careful coverage calibration was done for both PLD deposited Fe and Cu films separately at submonolayer thicknesses by taking STM images at different points of the RHEED oscillations to ascertain whether the maxima in RHEED amplitudes do correspond to one full monolayer or not. The necessity of this rather tedious coverage estimation procedure is due to the fact that, for thermally deposited Fe films the medium-energy electron-diffraction oscillations²³ show the first maximum only for 2 ML coverage since the first two layers do not grow layer-by-layer. Contrary to that for the pulsed laser deposited films the individual growth mode of both Fe and Cu layers proceeds in a layer-by-layer fashion. A KrF excimer laser ($\lambda = 248$ nm) with a fluence of 5 J/cm^2 , a pulse length of 34 ns and a repetition rate of 5–7 Hz was employed for depositing the Fe and Cu monolayers alternately. The average deposition rate has been established by setting the laser pulse repetition rate and ranges from 0.25 to 0.33 ML/min whereas the instantaneous deposition rate during a single pulse is controlled by the laser fluence and reaches approximately 10^5 ML/min, estimated from the pulse duration taking into account a certain decay time of the plasma plume. Thus, within a single laser shot about 1/1000 of a monolayer is actually being deposited. [For comparison: Thermal deposition experiments of Fe on Cu (Ref. 20) report typical average=instantaneous deposition rates of 0.33–0.5 ML/min]. The pressure in the UHV chamber during the PLD deposition has been kept below 5×10^{-10} mbar.

Figure 2 shows typical RHEED oscillations for a 6 ML Fe-Cu stacking. The first maximum corresponds to 1 ML Fe and the second maximum corresponds to the second layer completion by 1 ML Cu. At each maximum (as marked with arrows) the laser target was changed manually within 6–10 s. To maintain the required precision in layer filling during the whole course of multilayer stacking the average deposition rate had to be kept at about 200 s per 1 monolayer. Note that the deposition at room temperature results in a continuous decrease of the RHEED intensity although the layer-by-layer sequential filling is maintained. Deposition at elevated substrate temperatures was avoided because of possible mutual interdiffusion of Fe and Cu leading to mixed interfaces although it would improve the surface ordering. The RHEED oscillations disappear when the total thickness approaches 50 ML which coincides with the fcc to bcc structural transition (see below).

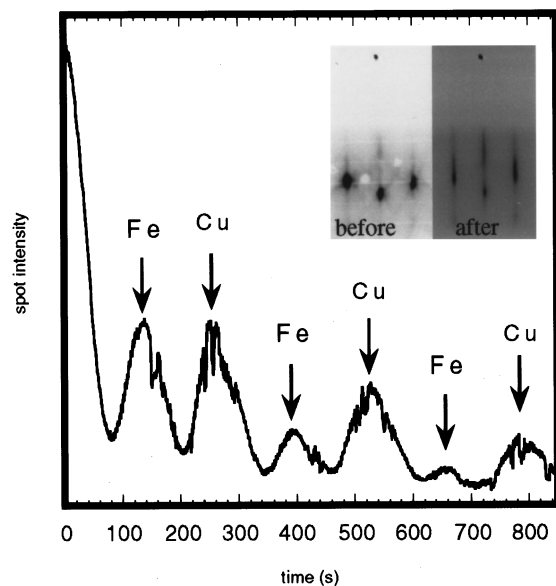


FIG. 2. Typical RHEED oscillations for a 6 ML Fe-Cu stacking on Cu(001) prepared by the PLD method. The first maximum corresponds to 1 ML filling of Fe and the second maximum to the filling of the next layer, i.e., 1 ML of Cu, and so forth. Inset: RHEED pattern before and after deposition.

Morphological studies from STM images

Figures 3(a)–3(d) show the surface morphology of the room-temperature-deposited multilayers. The STM images for each monolayer coverage were recorded on samples after

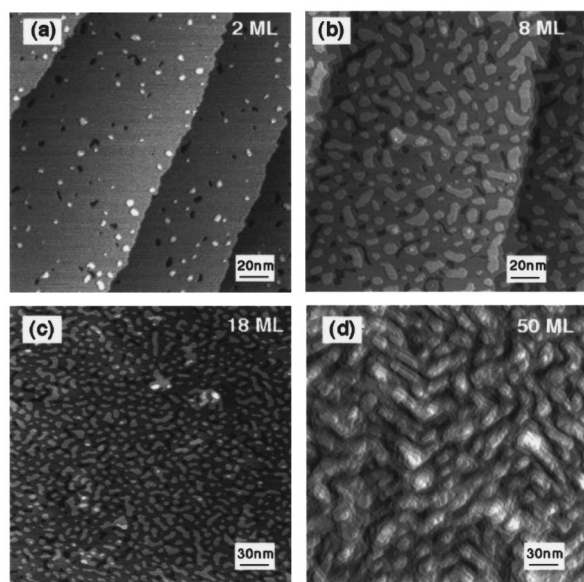


FIG. 3. Surface topography of Fe-Cu multilayers deposited on Cu(001) at room temperature. All STM images were taken in the constant current mode with sample bias of +0.5–+1.0 V and a tunneling current of about 1 nA. (a) A 2 ML Fe-Cu film shows an almost complete second layer (Cu, grey) coverage with very insignificant parts of first layer (Fe, black), and third layer (Cu, white) exposed. (b) and (c) 8 and 18 ML films show a nearly layer-by-layer filling with only three topmost monatomic levels visible. (d) A 50 ML film changes to a ridgelike morphology of enhanced roughness with two 90° oriented domains.

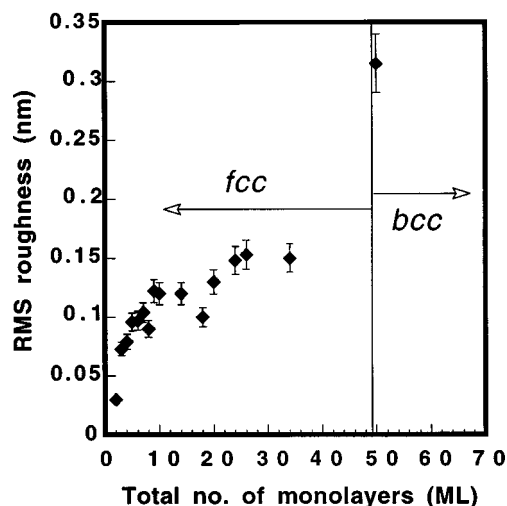


FIG. 4. Plot of root mean square (rms) roughness versus monolayer thickness as measured by STM. After an initial increase the roughness seems to approach an average of 0.14 nm.

performing MOKE measurements. Accordingly each film has been exposed to thermal cycles in the temperature range from 160 up to 450 K. In Fig. 3(a) the small black regions correspond to the first deposited monolayer, i.e., Fe. Grey regions correspond to Cu, the second ML. The analysis indicates that >98% of the first monolayer (Fe) is covered by the second layer (Cu). An insignificant part of the first monolayer (<2%) remains exposed. A small coverage (<2%) of Cu appearing as a third layer is evident from the whiter islands which are visible. Figure 3(b) shows the situation for an 8 ML film ($n=4$ bilayers), where the top layer is Cu. Although the difference in flatness between the 2 and 8 ML films is evident, the growth mode is still layer-by-layer since there are obviously only three monatomic levels present. As we proceed 18 ML [$n=9$ bilayers, Fig. 3(c)] the morphology changes only a little. The average island size around 18 ML becomes smaller. A comparison of Figs. 3(a)–3(c) and 3(d) shows that a structural transition has occurred for a 50 ML ($n=25$ bilayers) coverage. A closer look at the morphology of Fig. 3(d) shows a ridgelike appearance (90° oriented islands) of this 50 ML film. A similar ridgelike morphology has been observed for thermally deposited Fe on Cu(001) after the structural phase transition from fcc to bcc.²⁰ From the measured thickness series we conclude that in our metastable, ordered FeCu alloy the fcc to bcc transformation occurs between 44 ($n=22$ bilayers) and 50 ML.

The (rms) surface roughness during the monolayer stacking is shown as a function of total number of monolayers (Fe and Cu alternately) in Fig. 4. The roughness tends to increase between 2 and 10 ML and thence it seems to fluctuate around an average value of 0.14 nm. This trend in roughness involving a maximum of three monatomic levels at any time is consistent with the observed nearly layer-by-layer growth of RT grown films. The emerging roughness with increasing monolayer stacking has been a point of sustained research effort to identify the causes and consequences of surface roughening during epitaxial growth. Stochastic models²⁴ have been popular in the recent past, but mean-field theories²⁵ are adequate to describe the commonly observed types of surface roughening,²⁶ step bunching,²⁷ or three-

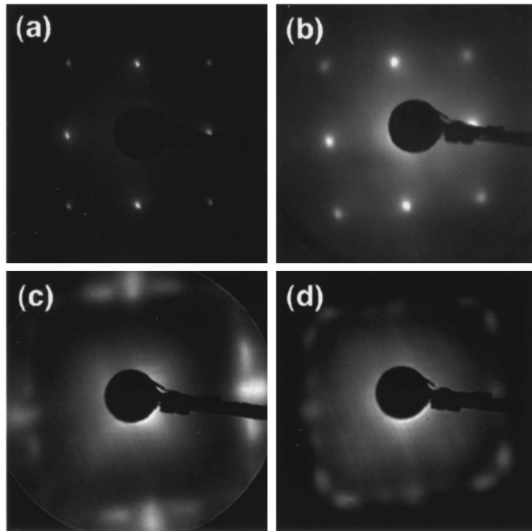


FIG. 5. LEED pattern (a) of a clean Cu(001) at 156 eV showing a $p(1 \times 1)$ structure, (b) of a 44 ML Fe-Cu multilayer stacking still showing a clear fcc long-range ordering (note the sharp spots), (c) and (d) of a 50 ML Fe-Cu film show a typical (3×1) reconstruction characteristic for a Pitsch orientation of a bcc lattice on an fcc lattice at 68.5 and 90 eV, respectively.

dimensional island formation associated with either misfit strain relief²⁸ or the presence of relatively high-energy barriers to interlayer atomic migration at step edges.²⁹ In the two alloy ordering experiments^{1,2} (as in the present case) roughening due to the strain relief seems to be more predominant than the step bunching mechanism. Therefore growth-induced roughening which is a consequence of morphological deviations from a flat surface profile seems to be inevitable during epitaxial growth. Upon the fcc \rightarrow bcc structural transformation the rms roughness increases drastically, from a value as low as 0.15 nm at 34 ML thickness to above 0.3 nm at 50 deposited monolayers.

LEED studies

The structural transformation from fcc to bcc around 50 ML coverage is further substantiated by LEED patterns as shown in Figs. 5(a)–5(d). Figure 5(a) shows the $p(1 \times 1)$ pattern of the clean Cu substrate observed subsequent to Ar⁺ sputtering and annealing at 873 K. It is noteworthy to compare the LEED pattern [Fig. 5(b)] obtained for a 44 ML film of Fe and Cu on Cu(001). The still sharp $p(1 \times 1)$ pattern is identical to that of the Cu substrate which confirms that the multilayer growth proceeds with an fcc structure. However a distinct change is noted for the 50 ML Fe-Cu film [Figs. 5(c) and 5(d)] which shows a (3×1) reconstruction characteristic for a Pitsch orientation³⁰ of the bcc lattice on the fcc lattice in (001) orientation. This is in accordance with the morphological change noticed from the STM image for 50 ML Fe-Cu film.

MAGNETIC PROPERTIES OF THE Fe-Cu MULTILAYERS

MOKE hysteresis loops recorded in longitudinal geometry are shown in Fig. 6 for a total of 6 ML = (Cu/Fe)₃/Cu(001) and in Fig. 7 for a total of

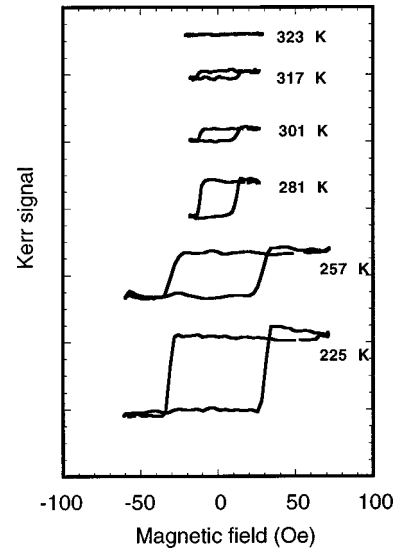


FIG. 6. MOKE hysteresis loops versus temperature for a 6 ML Fe-Cu film on Cu(001) measured in in-plane geometry.

20 ML = (Cu/Fe)₁₀/Cu(001) multilayer. Both figures show the temperature dependence of nearly rectangular hysteresis loops with an in-plane easy axis of magnetization while there is no component of spontaneous magnetization perpendicular to the film plane. The onset of this in-plane magnetization was measured for the basic unit of a double layer Cu/Fe on Cu(001) too, but only at a much lower temperature of 50 K. The coercivity, H_c of these films at low temperature is in the range of 15–30 Oe.

From the temperature dependence of the saturation magnetization (Figs. 6 and 7) the Curie temperature T_C for each multilayer stacking has been determined. The thickness dependence of T_C is shown in Fig. 8. The lowest T_C of a Fe-Cu multilayer stacking we measured was 225 K for 3 ML. For 2 ML ($n=1$ bilayer) only the onset of in-plane magnetization could be observed but for a T_C determination the signal was too low and unstable. In Fig. 8 we have added a T_C value of 110 K for 1 ML Fe on Cu(001) deposited at RT by PLD,

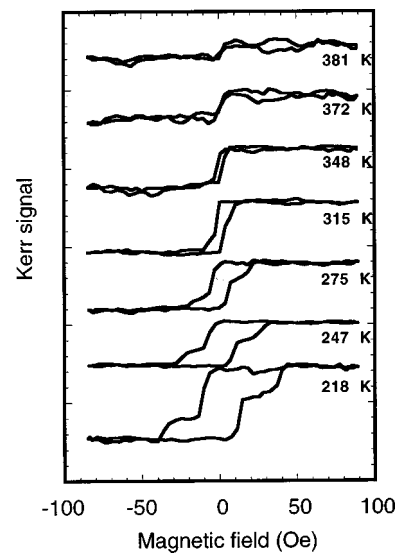


FIG. 7. Temperature dependence of in-plane hysteresis loops for a 20 ML Fe-Cu stacking on Cu(001).

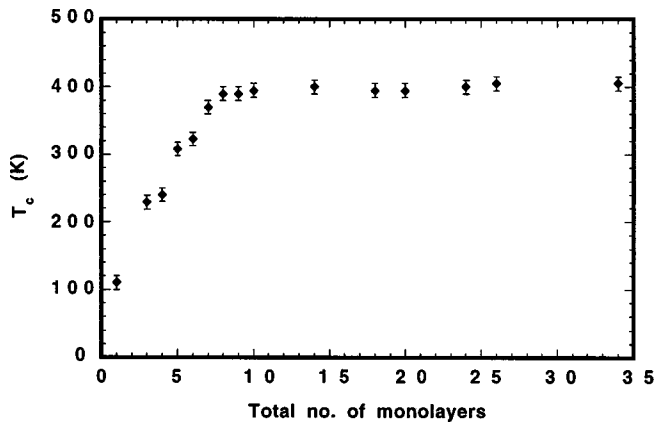


FIG. 8. Curie temperature T_C versus total number of Fe and Cu stacked layers on Cu(001).

taken from a unpublished study.³⁴ Extrapolating the measured T_C downwards we estimate a T_C for 2 ML of about 130 K. With increasing thickness T_C varies systematically. Up to 10 ML ($n=5$ bilayers) T_C continuously increases reaching a saturation value of 400 K. Between 10 and 34 ML ($n=17$ bilayers) T_C is practically constant and fluctuates around the average value of 400 K by ± 5 K. This value of T_C can be reproduced and determined without causing irreversible changes of the ordered alloy by interdiffusion. Above 34 ML, there is a large discontinuity in T_C and it exceeds above 500 K which is beyond our heating capability.

A plot of the measured MOKE signal at a fixed T/T_C ratio versus the number of stacked monolayers is presented in Fig. 9. The values are taken at reproducible optical conditions in the in-plane geometry and are consistent with a selected number of saturation values measured in standard polar geometry (near normal incidence) in the magnetically hard direction. Thus it became possible to compare the magnetization with earlier results on Fe grown on Cu(001) by thermal deposition and transformed into the bcc phase, which is known to assume the high spin state of $2.2 \mu_B$ per atom. Our metastable multilayer FeCu alloy exhibits a linear increase of its saturation with thickness reaching a value for the bcc transformed film at 50 ML (corresponding to 25 ML of pure Fe) which matches the extrapolation of the saturation measured for the 14 ML thermally deposited pure iron on

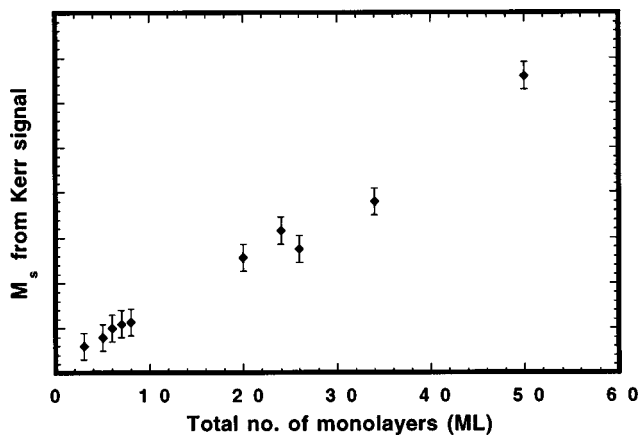


FIG. 9. Saturation magnetization as inferred from Kerr measurements in longitudinal geometry versus multilayer film thickness.

Cu(001) within the limits of accuracy of the present measurement ($\pm 10\%$).

DISCUSSION

Epitaxial ultrathin films of Fe on Cu(001) represent one of the most studied systems for magnetism in reduced dimensions because of the richness of different structural and magnetic phases depending on thickness as well as on experimental conditions.³² However, usual thermal deposition techniques at room temperature or low temperature do not result in a true 2D growth of the first monolayer which is a prerequisite for the fabrication of alternately stacked monolayers of Fe and Cu in an artificially ordered $L1_0$ phase. Therefore we employed PLD to force two-dimensional growth of alternate Fe and Cu monolayers at RT.³ RHEED oscillations (Fig. 2) recorded during growth and STM images [Figs. 3(a)–3(c)] prove, that stacked monatomic Fe-Cu multilayers grow almost in a perfect layer-by-layer mode from the beginning. Although with increasing thickness up to total of 34 ML the roughness of the surface increases, mainly three atomic levels are exposed at the same time. This is also evidenced by the measured rms surface roughness (Fig. 4) which increases monotonously between 2 and 10 ML and thence fluctuates around 0.14 nm involving a maximum of three atomic levels. Up to almost 50 ML overall thickness RHEED oscillations and STM images do not show any morphological changes, that means a constant growth of an ordered superlattice. At 50 ML a drastic change in surface morphology is observed [Fig. 3(d)]. The formation of ridgelike 90° -oriented islands of substantially higher roughness indicate a structural transformation from fcc to bcc in this thickness region.

This fcc to bcc transformation is proved by LEED (Fig. 5). The $p(1 \times 1)$ pattern of the clean fcc Cu(001) substrate is maintained up to total of 44 ML with no visible deterioration of the sharpness of the spots. This indicates that the stable two-dimensional growth mode of atomic multilayers results in a perfect fcc structure.

However, around 50 ML thickness the LEED pattern [Figs. 5(c) and 5(d)] suddenly changes to a (3×1) reconstruction. This can be interpreted by a structural phase transition from fcc multilayers to bcc multilayers or Fe precipitates. The (3×1) LEED pattern corresponds to a Pitsch orientation in which (011) planes are parallel to (001) fcc planes and one $[112]$ bcc overlayer direction parallel to $\langle 110 \rangle$ fcc substrate directions.^{29,32} This structural phase transition manifests itself also in the sudden change in the morphology from a nearly layer-by-layer growth to a ridgelike appearance consisting of two 90° -oriented domain systems with a remarkably increased roughness. Why the structural transition from $L1_0$ to bcc just arises near 50 ML thickness is not known. One can speculate that with a mean roughness of three atomic levels at the surface as well as in the buried layers of the multilayer system the probability of short circuits between adjacent Fe layers increases with the film thickness. Short circuits mean local percolations of Fe layers normal to the layer stacking at which the transition from the $L1_0$ structure to the bulk bcc Fe phase could start far below 50 ML. At around 50 ML the structure of the surface layers then becomes predominantly bcc. The morphological and

structural studies can be summarized to give a consistent picture of a metastable ordered $L1_0$ phase of the artificial FeCu alloy up to about 50 ML by employing the PLD method to enforce an improved layer-by-layer growth.

To start the discussion of the magnetic properties of the artificial fcc FeCu alloy we remind the reader that although the Fe-Cu(001) system is well investigated it is one of the most complex magnetic ultrathin film systems. By employing PLD as a deposition method we add aspects to the already known richness of structural and magnetic phases.³³ A 1 ML Fe film on Cu(001) deposited by PLD at RT (which cannot be produced by thermal deposition because of the initial bilayer growth mode) shows an out-of-plane magnetization as measured by MOKE in polar geometry.³⁴ In a theoretical calculation³⁵ this perpendicular magnetic anisotropy was predicted to hold up to 4 ML Fe and with decreasing anisotropy switches to in-plane anisotropy at around 8 ML Fe. This behavior could be confirmed by PLD deposited Fe films³³ however, the spin reorientation already occurs at 2 ML. In another calculation of magnetic anisotropy energies in the Fe-Cu(001) system³⁶ the always positive band energy favoring the perpendicular orientation of magnetization was found to be too small to compensate the negative contribution of the magnetostatic dipole-dipole energy, therefore an in-plane magnetization was predicted for any Fe layer thickness. This contradicts the theoretical result of Ref. 35 as well as our finding below 2 ML.³⁴ 1 ML Fe covered by 1 ML Cu represents the basic unit of a bilayer of our artificially ordered alloy stacking for which we measured the onset of an easy axis of in-plane magnetization. This is contrary to the predictions of out-of-plane magnetization for the Fe-Cu double layer of both theoretical calculations.^{35,36} Once the in-plane magnetization is established in the basic unit one would not expect any change in the direction of magnetization because of the increasing influence of the shape factor and the decreasing influence of the interface anisotropy. Indeed we measure clear in-plane loops (Figs. 6 and 7) with full remanence and relatively small coercivities of 15–30 Oe up to a thickness of 34 ML. The change from out-of-plane easy axis for 1 ML bare Fe to the in-plane easy axis for the bilayer unit (1 ML Fe capped by 1 ML Cu) indicates the strong influence of a nonmagnetic capping layer on anisotropy which was found also in other systems.³⁷

The thickness dependence of the Curie temperature (Fig. 8) clearly shows the general behavior of linear increase and saturation correlated to the reduced dimensionality in ultrathin films.³⁸ The saturation value of 400 K already achieved

at 10 ML ($n=5$ bilayers) and then remaining constant up to 34 ML in our *single-crystalline* epitaxial alloy matches with an earlier result for a Fe₅₀Cu₅₀ *polycrystalline* alloy film deposited by high rate sputtering.¹⁰

Up to a thickness of 34 ML the magnetic properties correlate with the morphological and structural properties, i.e., a layer-by-layer grown artificially ordered FeCu alloy with an fcc $L1_0$ structure shows one ferromagnetic phase with a uniform in-plane easy axis of magnetization. The nature of the magnetic phase between 35 and 50 ML is not known, however, beyond 50 ML the high T_C of above 500 K is correlated with the stable bcc Fe structure.

From the linear behavior of the saturation magnetization (Fig. 9) one can also conclude about a single magnetic state of the Fe atoms within the whole thickness range between 2 and 34 ML ($n=1-17$ bilayers), the magnitude of which corresponds to the high moment state of bulk bcc Fe.

SUMMARY

Multilayers of a metastable fcc FeCu alloy in the $L1_0$ structure were produced using pulsed-laser deposition by stacking one monolayer of Fe and one monolayer of Cu alternately onto Cu(001). Morphological studies by RHEED oscillation measurements and STM images indicate that the ordered Fe-Cu multilayers grow in a nearly perfect layer-by-layer mode with an initially increasing but then constant roughness involving a maximum of three monatomic levels. Multilayers up to 44 ML thickness have fcc structure as proved by LEED. Starting with the basic unit of one Fe-Cu bilayer up to a thickness of 34 ML ($n=17$ bilayers) magneto-optical Kerr effect measurements (MOKE) show ferromagnetic hysteresis loops with an in-plane easy axis of magnetization. The coercivity remains as low as 15–30 Oe. The Curie temperature T_C increases linearly from about 130 K at 2 ML ($n=1$ bilayer) to the saturation value of 400 K at 10 ML ($n=5$ bilayers). Above 44 ML the surface morphology changes to a ridgelike appearance connected with a drastic increase of roughness for which LEED pattern reveal a structural transition from fcc into bcc with a Pitsch orientation, at the same time T_C jumps up beyond 500 K at 50 ML thickness.

ACKNOWLEDGMENTS

The authors thank G. Kroder and F. Pabisch for their technical support. S.S.M. thanks the Max Planck Society for financial support.

*Permanent address: Department of Chemistry, Indian Institute of Technology Kanpur, 208 016 INDIA; Electronic address: ssundar@iitk.ernet.in

¹K. Takahashi, S. Mitani, M. Sano, H. Fujimori, H. Nakajima, and A. Osawa, *Appl. Phys. Lett.* **67**, 1016 (1995).

²S. Mitani, K. Takahashi, M. Sano, H. Fujimori, A. Osawa, and H. Nakajima, *J. Magn. Magn. Mater.* **148**, 163 (1995).

³S. Sundar Manoharan, J. Shen, M. Klaua, H. Jenniches, and J. Kirschner, *J. Appl. Phys.* **81**, 3768 (1997).

⁴E. F. Kneller, *J. Appl. Phys.* **35**, 2210 (1964); **33**, 1355 (1962).

⁵J. Friedel, *Nuovo Cimento Suppl.* **7**, 287 (1958).

⁶J. T. Norton, *Trans. Metall. Soc. AIME* **116**, 386 (1935).

⁷L. S. Darken and H. A. Wriedt, *Trans. Metall. Soc. AIME* **218**, 30 (1960).

⁸J. W. Klement, *Trans. Metall. Soc. AIME* **233**, 1180 (1965).

⁹K. Sumiyama, T. Yoshitabe, and Y. Nakamura, *J. Phys. Soc. Jpn.* **53**, 2160 (1984).

¹⁰C. L. Chien, S. H. Liou, D. Kofalt, Wu Yu, T. Eqami, and T. R. McGuire, *Phys. Rev. B* **33**, 3247 (1986).

¹¹P. Crespo, A. Hernando, A. R. Yavari, O. Drbohlár, A. G. Escorial, J. M. Baranidaran, and I. Orue, *Phys. Rev. B* **48**, 7134 (1993).

¹²T. Ambrose, A. Gavrin, and C. L. Chien, *J. Magn. Magn. Mater.* **124**, 15 (1993).

- ¹³V. G. Harris, K. M. Kemmer, B. N. Das, N. C. Koon, A. E. Ehrlich, J. P. Kirkland, J. C. Woicik, P. Crespo, A. Hernando, and A. G. Escorial, *Phys. Rev. B* **54**, 6929 (1996).
- ¹⁴K. Uenishi, D. F. Kobayashi, K. N. Ishihara, and P. H. Shingu, *Jpn. J. Appl. Phys., Part 2* **30**, L854 (1991).
- ¹⁵K. Uenishi, K. F. Kobayashi, S. Nasu, H. Hatano, K. N. Ishihara, and P. H. Shingu, *Z. Metallkd.* **83**, 132 (1992).
- ¹⁶A. R. Yavari, P. J. Desre, and T. Benameur, *Phys. Rev. Lett.* **68**, 2235 (1992).
- ¹⁷W. B. Pearson, *Handbook of Lattice Spacing and Structure of Metals and Alloys* (Pergamon, New York, 1958), p. 602.
- ¹⁸V. L. Moruzzi, P. M. Markus, and J. Kuebler, *Phys. Rev. B* **39**, 6957 (1989).
- ¹⁹J. Shen, J. Giergiel, A. Schmid, and J. Kirschner, *Surf. Sci.* **328**, 32 (1995).
- ²⁰J. Giergiel, J. Shen, J. Woltersdorf, A. Kirilyuk, and J. Kirschner, *Phys. Rev. B* **52**, 8528 (1995).
- ²¹H. Jenniches, M. Klaua, H. Hoeche, and J. Kirschner, *Appl. Phys. Lett.* **69**, 339 (1996).
- ²²OMICRON CMA150™, Taunusstein, 1985.
- ²³D. A. Steigerwald, I. Jacob, and W. F. Egelhoff, Jr., *Surf. Sci.* **202**, 472 (1988).
- ²⁴J. Villain, *J. Phys. I* **1**, 19 (1991).
- ²⁵P. I. Cohen, G. S. Petrich, P. R. Pukite, G. J. Whaley, and A. S. Arrot, *Surf. Sci.* **216**, 222 (1989).
- ²⁶D. E. Jesson, S. J. Pennycook, J. Z. Tischles, J. D. Budai, J. M. Baribeau, and D. C. Houghton, *Phys. Rev. Lett.* **70**, 2293 (1993); G-B. Stringfellow, L. C. Su, Y-E. Strausses, and J. T. Thornton, *Appl. Phys. Lett.* **66**, 3155 (1995).
- ²⁷A. A. Chernov, *Modern Crystallography III* (Springer-Verlag, Berlin, 1984).
- ²⁸D. J. Eaglesham and M. Cerullo, *Phys. Rev. Lett.* **64**, 1943 (1990).
- ²⁹J. R. Smith, Jr. and A. Zangwill, *Phys. Rev. Lett.* **76**, 2097 (1996).
- ³⁰W. Pitsch, *Philos. Mag.* **4**, 577 (1959).
- ³¹W. Kuch, M. Salviati, Xingyu Gao, M. T. Lin, M. Klaua, J. Barthel, Ch. V. Mohan, and J. Kirschner, following paper, *Phys. Rev. B* **58**, 8556 (1998).
- ³²M. T. Kief and W. F. Egelhoff, Jr., *Phys. Rev. B* **47**, 10 785 (1993).
- ³³H. Jenniches, J. Shen, Ch. V. Mohan, S. Sundar Manoharan, J. Barthel, Ph. Ohresser, M. Klaua, and J. Kirschner (unpublished).
- ³⁴Ch. V. Mohan, J. Shen, P. Ohresser, M. Zheng, M. Klaua, J. Barthel, and J. Kirschner (unpublished).
- ³⁵R. Lorenz and J. Hafner, *Phys. Rev. B* **54**, 15 937 (1996).
- ³⁶B. Ujfalussy, L. Szunyogh, and P. Weinberger, *Phys. Rev. B* **54**, 9883 (1996).
- ³⁷F. O. Schumann, M. E. Buckley, and J. A. C. Bland, *J. Appl. Phys.* **76**, 6093 (1996); B. N. Engel, M. H. Wiedmann, R. A. Van Leeuwen, and C. M. Falco, *Phys. Rev. B* **48**, 9894 (1993); W. Weber, C. H. Back, U. Ramsperger, A. Vaterlaus, and R. Allenspach, *ibid.* **52**, R14 400 (1995).
- ³⁸C. M. Schneider, P. Bressler, P. Schuster, and J. Kirschner, *Phys. Rev. Lett.* **64**, 1059 (1990).